Spectroscopic second-harmonic generation during Ar^+-ion bombardment of Si(100)

J. J. H. Gielis, P. M. Gevers, A. A. E. Stevens, H. C. W. Beijerinck, M. C. M. van de Sanden, and W. M. M. Kessels*
Department of Applied Physics, Eindhoven University of Technology, P.O. Box 513, 5600 MB Eindhoven, The Netherlands
(Received 27 February 2006; revised manuscript received 18 May 2006; published 10 October 2006)

Spectroscopic and real time optical second-harmonic generation (SHG) has been applied to gain insight into the surface and interface processes during low-energy (70–1000 eV) Ar^+-ion bombardment of *H* terminated Si(100). The Ar^+-ion bombardment of the crystalline silicon (*c*-Si), which creates a layer of amorphous silicon (*a*-Si), has been studied in the SH photon energy range of 2.7–3.5 eV. The time-resolved SHG signal has been observed to increase with an order of magnitude upon ion bombardment. Spectroscopic SHG during ion bombardment and after subsequent XeF_2 dosing indicates that the SHG signal has both a contribution generated at the buried interface between the *a*-Si and the *c*-Si and an additional contribution originating from the *a*-Si surface. By separating these contributions using a critical point model it has been shown that the SHG spectra consist of a sharp resonance at 3.36 eV with a linewidth of 0.1 eV at the buried *a*-Si/*c*-Si interface and a much broader resonance at a resonance energy of 3.2 eV with a linewidth of 0.5 eV at the *a*-Si surface. The former resonance is identified to originate from E_0'/E_1 transitions between bulk electronic states in the *c*-Si that are modified due to the vicinity of the interface, while the latter resonance is caused by transitions related to Si-Si bonds in the surface region of the *a*-Si. The time-resolved dynamics of the SHG signal can help in understanding the mechanism of ion-beam and plasma etching of silicon.

DOI: 10.1103/PhysRevB.74.165311 PACS number(s): 78.68.+m, 42.65.Ky, 52.77.−j, 73.20.At

I. INTRODUCTION

Dry etching or plasma etching is a key technology in the manufacturing of integrated circuits, microelectromechanical systems (MEMS), and optoelectronic devices. The main advantage of plasma etching compared to chemical wet etching is the ability to etch anisotropically and thereby creating high aspect-ratio structures. This important characteristic of plasma etching is caused by the directionality of ions present in the plasma, which arises as the ions are accelerated by the relatively large electric fields present in the boundary layer, the so-called sheath, between the plasma and the substrate. The ions can reach energies on the order of 10–1000 eV depending on the plasma configuration and operation conditions. In addition, the synergy between the ions and the, usually halogen based, etchants in the plasma enhances the anisotropy and induces a high etch rate.[1] However, as lithography techniques improve and feature sizes in new generation devices continuously shrink, etching technology has to keep up with the same trend. Therefore, etching equipment and processes have to be improved for the next-level of process control. In general, such improvements are based on empirical observations. However, it would be beneficial to have profound understanding of the plasma etching mechanism. Therefore, numerous fundamental studies have been performed within the last decades leading to a detailed picture of the reaction mechanisms involved, as reviewed by Winters and Coburn.[2] One of the main difficulties of such studies is the complex chemistry inherent to the plasma environment. To circumvent these problems, the plasma is often "mimicked" by beam etching experiments. Also molecular dynamics (MD) and Monte Carlo simulations have proven their value in the description of the plasma etching process.[3–5]

In this work we use a unique approach to study the role of ion bombardment in the etching process of crystalline silicon (*c*-Si) by applying the nonlinear optical technique of second-harmonic generation (SHG) in a beam experiment. Here we focus on SHG during Ar^+-ion bombardment of Si(100), but it is expected that the results have also implications for understanding ion-enhanced etching with halogen-based etchants. Ion bombardment of *c*-Si induces the formation of a damaged layer of amorphous silicon (*a*-Si). Moreover, it also cleans the *a*-Si surface by sputtering. For this reason the technique of ion bombardment, in combination with a recrystallization anneal, is also widely used for cleaning Si surfaces, e.g., for native oxide removal.[6–8] The properties of the surface of the *a*-Si and the buried interface between the *a*-Si and the underlying *c*-Si can reveal different aspects of the plasma etching mechanism. Moreover, the decreasing device dimensions inherently augment the influence of surface and interface properties on device performance. In this respect, the surface and interface sensitive technique of SHG might be beneficial to the understanding of plasma etching and the resulting material properties.

Within the electric dipole approximation, SHG is described by a second-order nonlinear polarization $\mathbf{P}^{(2)}(2\omega)$ in a medium induced by an incident electric field $\mathbf{E}(\omega)$ (Ref. 9)

$$\mathbf{P}^{(2)}(2\omega) = \varepsilon_0 \vec{\chi}^{(2)}(2\omega):\mathbf{E}(\omega)\mathbf{E}(\omega), \tag{1}$$

where $\vec{\chi}^{(2)}(2\omega)$ is the second-order nonlinear susceptibility tensor. SHG is forbidden in the bulk of centrosymmetric materials, such as *c*-Si and *a*-Si, as in these media symmetry considerations imply $\vec{\chi}^{(2)}=0$. However, at a surface or interface the symmetry is broken and $\vec{\chi}^{(2)}$ is nonzero, thereby making the technique of SHG particularly surface and interface sensitive. Microscopically, SHG is the conversion of two photons with energy $\hbar\omega$ into a single photon with energy $2\hbar\omega$. The process of SHG is resonantly enhanced when the photon energy of either the fundamental or the SH radiation coincides with the energy of an optical transition. Conse-

quently, SHG is a technique that is sensitive to both the symmetry and the electronic states of surfaces and interfaces. Moreover, being an optical technique, SHG is applicable *in situ* and is nonintrusive for low radiation fluence.

SHG has been applied extensively to study the Si/SiO_2 interface,[10] also in etching or ion bombardment related experiments of the Si/SiO_2 system.[11–13] Also the surface of clean and *H* terminated *c*-Si has been studied thoroughly with SHG.[14–20] In these studies the SHG signal from the *c*-Si surface has been shown to be sensitive to surface Si dangling bonds for photon energies in the range of ~1.0 to ~1.3 eV.[15,16,19] Furthermore, resonant features have been observed at a SH photon energy of ~3.4 eV. Based on the similarity in the location, these features have been identified to be related to the E_0'/E_1 critical point transitions of bulk *c*-Si that are modified due to the vicinity of the surface.[21] This modification has been suggested to cause distorted bonds at the surface[14] or a dc-electric field at the surface resulting in electric-field-induced SHG (EFISH).[18] SHG experiments in Si etching related studies have been reported by Haraichi and coworkers, who modified the surface of Si(111) by XeF_2 exposure.[22] Heinz *et al.* performed SHG experiments during ion bombardment of *c*-Si.[23] They observed decreasing anisotropic SHG contributions in Si(111)-7×7 during bombardment with 5 keV Ar^+ ions at a fixed SH photon energy of 2.33 eV. Here, we report on SHG experiments on Si(100) under bombardment of Ar^+ ions with energies in the range of 70–1000 eV, an energy range that is more relevant for plasma etching. We performed both real time and spectroscopic SHG experiments at SH photon energies between 2.7 and 3.5 eV, before, during, and after ion bombardment. Additionally, we modified the surface of the *a*-Si top layer by XeF_2 dosing. The SH photon energy range applied here has been selected as it includes the E_0'/E_1 critical point energies of bulk *c*-Si.[21]

This paper is organized as follows: In Sec. II the details of the high vacuum system, the silicon samples, and the optical setup will be addressed. In Sec. III we first briefly summarize the results of spectroscopic ellipsometry experiments, performed to characterize the *a*-Si layers. Next, in Sec. IV, the results of both real time and spectroscopic SHG experiments before, during, and after ion bombardment of *c*-Si are presented. These results are analyzed and discussed in Sec. V, using a critical point model.

II. EXPERIMENTAL DETAILS

A. High vacuum system and *in situ* diagnostics

The SHG experiments to study the etching process of *c*-Si were performed *in situ* in a high vacuum multiple-beam experiment. A schematic picture of this vacuum setup is shown in Fig. 1 together with the laser system and the optical setup. The sample is placed in a rotatable sample holder that allows for fast and reproducible sample replacement using a load lock and a linear magnetic drive. The sample holder can be heated, however the present experiments were carried out at room temperature. The sample chamber and the load lock, separated by a valve, are pumped by turbo molecular pumps to a base pressure below 10^{-8} mbar. The vacuum system is

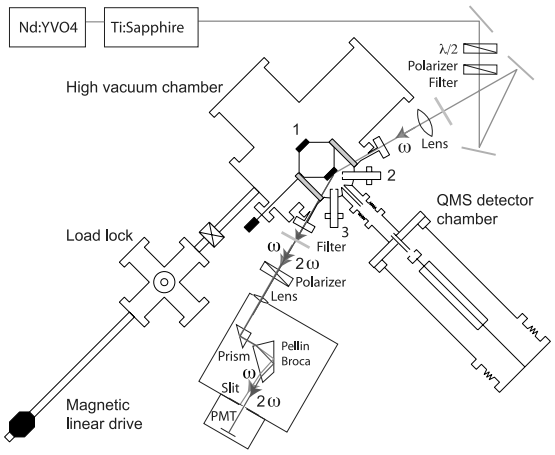

FIG. 1. Horizontal cross section of the high vacuum chamber and the optical setup. The samples are placed in a rotatable sample holder (1) and can be replaced using a load lock. The Ar^+-ion gun (2) and the XeF_2 source (3) are placed at 45° and 52° with respect to the sample surface normal. The fundamental laser radiation, provided by a Ti:sapphire laser, and the generated SH radiation propagate through the setup at 74° angle of incidence with respect to the sample surface normal. Detection of the SH radiation takes place by a photomultiplier tube (PMT) connected to photon counting electronics.

described in detail elsewhere.[24–26] The vacuum chamber is equipped with a XeF_2 source producing a beam that impinges at 52° angle of incidence with respect to the sample surface normal. Recently, a commercial low-energy ion gun (Nonsequitur Technologies, customized version of model LEIG-2), operated on Ar source gas with a purity of 99.999%, was added to the setup. This ion gun produces a beam of Ar^+ ions with energies tunable between 20 eV and 2 keV impinging at 45° angle of incidence at the sample. The spot size of the ion beam at the sample was set to ~5 mm^2, which exceeded the dimensions of the laser spot by more than 2 orders of magnitude. For all ion energies used in this study the applied ion flux was ~0.07 ML/s (1 ML=6.86×10^{14} cm^{-2}).

It is important to note that the SHG signal during ion bombardment is not influenced by surface contamination from background species, such as oxygen. The flux of background species at the sample is lower than 0.004 ML/s, as can be calculated from the base pressure of the high vacuum setup (10^{-8} mbar) using kinetic theory. As not all background species are reactive, the flux of species that will adsorb at the surface is even lower. The Ar^+-ion flux applied in this study, 0.07 ML/s, is over an order of magnitude higher than the flux of background species and results, e.g., for 1000 eV Ar^+ ions in a silicon sputter rate of 0.2 ML/s. Consequently, during ion bombardment any background species arriving at the surface will immediately be removed by sputtering.

The setup includes a quadrupole mass spectrometer (QMS) to determine the type and amount of species leaving the sample after interaction with the ion and/or XeF_2 beam and to perform residual gas analysis. To monitor the linear optical properties of the sample in real time during etching,

the optical technique of spectroscopic ellipsometry (SE) was used. Apart from the linear optical properties of the sample, in the present case the *a*-Si/*c*-Si system, SE provided the thickness and the surface roughness of the *a*-Si layer. The SE experiments were carried out in separate studies with a J.A. Woollam, Inc. M2000U rotating compensator ellipsometer with infrared extension covering the photon energy range of 0.75–5 eV.[27] The SE measurements were performed using the same view ports in the vacuum system as used for the SHG measurements and under identical etching conditions as used in the SHG experiments. The SE data are analyzed using a three-layer optical model describing the *c*-Si substrate, a layer of *a*-Si, and a surface roughness layer that is modeled as an effective medium consisting of 50% voids and 50% *a*-Si using the Bruggeman approximation. The dielectric function of the *a*-Si layer is parametrized using the Tauc-Lorenz formalism.[28]

B. Sample preparation

The experiments were performed with *H* terminated Si(100) samples (*n* type, phosphorus doped, resistivity 10–30 Ω cm). The preparation of these samples consisted of rinsing with ethanol and acetone, followed by ultrasound cleaning in an ethanol bath and finally immersion in a 2% HF solution for 2 min. Directly after HF treatment the samples were transferred into the load lock of the high vacuum setup, preventing the reformation of a native oxide. The samples were oriented at an azimuthal angle of 45° with respect to the [001] crystal axis.

C. Laser and optical setup

The fundamental laser radiation used for the SHG experiments had a photon energy tunable between 1.35–1.75 eV, a pulse duration of ~90 fs, and a repetition rate of 80 MHz. These light pulses were provided by a Ti:sapphire oscillator [Spectra Physics (SP) Tsunami] with broadband optics pumped by an intracavity doubled continuous wave $Nd:YVO_4$ laser (SP Millennia Vsj). The laser beam was guided to the sample in the high vacuum setup with broadband silver coated mirrors [New Focus (NF) 5103]. A variable wave plate (NF 5540) and a Glan-Thompson polarizer (NF 5525) were used to select the desired polarization of the radiation and to set the power of the laser beam at the sample to typically 50 mW. Any radiation at the SH wavelength generated in the laser or in optical components in the beam path was suppressed by a factor of $>10^4$ using a color filter (Schott OG 570). The fundamental beam entered the vacuum chamber through a stress free fused silica view port and was focused onto the sample to a spot with a radius of ~100 μm using a BK7 lens (CVI PLCX 25.4-103.0-C). With an angle of incidence at the sample of 74° with respect to the surface normal, this led to a typical fluence of ~2 $\mu J/cm^2$ per pulse. After leaving the vacuum chamber through another fused silica view port, the reflected beam passed a second polarizer (Thorlabs GL10A) to select the desired polarization direction and two color filters (Schott BG40) to suppress the fundamental radiation by a factor of $>10^6$. After separating the SH and the remaining fundamental radiation spatially using a Pellin Broca dispersion prism, the beam was focused with a lens (CVI PLCX 25.4-64.4-C) onto a slit placed in front of a photomultiplier tube (Hamamatsu R585). The photomultiplier tube was connected to photon counting electronics to record the SHG signal. The dark count rate of this detection scheme was below 4 Hz.

The SHG intensity is proportional to the magnitude of the second-order nonlinear susceptibility squared and to the square of the intensity of the fundamental radiation, $I_{in}(\omega)$, as can be derived from Eq. (1)

$$I(2\omega) \propto |\mathbf{P}^{(2)}(2\omega)|^2 \propto \varepsilon_0^2 |\vec{\chi}^{(2)}(2\omega)|^2 I_{\text{in}}^2(\omega). \tag{2}$$

The SHG intensity has been calculated from the measured SHG signal after correction for the laser intensity and the response of the optical system. The transmission of the optics was calibrated in separate transmission measurements. In addition, the transmission of the optics and the response of the photomultiplier tube were verified using the SHG signal generated on a single-side polished *z*-cut quartz sample replacing the sample. The second-order relation between laser intensity and SHG intensity was verified for all types of samples. In this paper two types of SHG experiments are reported: (1) real time SHG experiments carried out at a fixed wavelength during sample modification and (2) spectroscopic SHG measurements performed under steady-state conditions. The SHG intensity obtained in the spectroscopic experiments will be represented as a function of the SH photon energy. All results presented here are obtained at *p* polarized fundamental and SH radiation, as this polarization setting resulted in the highest signal (~70 times higher) compared to other polarization configurations.

III. SPECTROSCOPIC ELLIPSOMETRY RESULTS

First, we briefly address some results obtained by spectroscopic ellipsometry (SE) that are relevant for the interpretation of the SHG experiments. More details are reported elsewhere.[27] The *a*-Si layers studied with SE were generated with 70, 200, and 1000 eV Ar^+ ions and the data could be modeled with the same Tauc-Lorenz parameters for all *a*-Si layers, independent of the ion energy used. Consequently, the linear optical properties of the *a*-Si layers generated with different ion energies can be assumed to be equal. Figure 2(a) shows the photon energy dependence of the refractive index *n* and the extinction coefficient *k* of the *a*-Si layers, as calculated from the Tauc-Lorenz parameters. As a reference the values of *n* and *k* for a *c*-Si sample are also shown.[28] From the index of refraction and the extinction coefficient the linear susceptibility squared $|\chi^{(1)}|^2$ can be calculated with $|\chi^{(1)}|^2=(n^2-k^2-1)^2+(2nk)^2$. The resulting linear susceptibilities squared $|\chi^{(1)}|^2$ for *a*-Si and *c*-Si, which reflect the bulk optical properties of the material, can be compared to the second-order nonlinear susceptibility squared $|\chi^{(2)}|^2$ or SHG intensity obtained from the experiments. This comparison might provide information on the origin of the SHG signal. For the *a*-Si layers a single broad peak at a photon energy of ~3.2 eV is found in $|\chi^{(1)}|^2$, as is shown in Fig. 2(b). Conversely, $|\chi^{(1)}|^2$ for *c*-Si displays two sharp features at 3.37 eV and 4.3 eV, of which the former is related to the

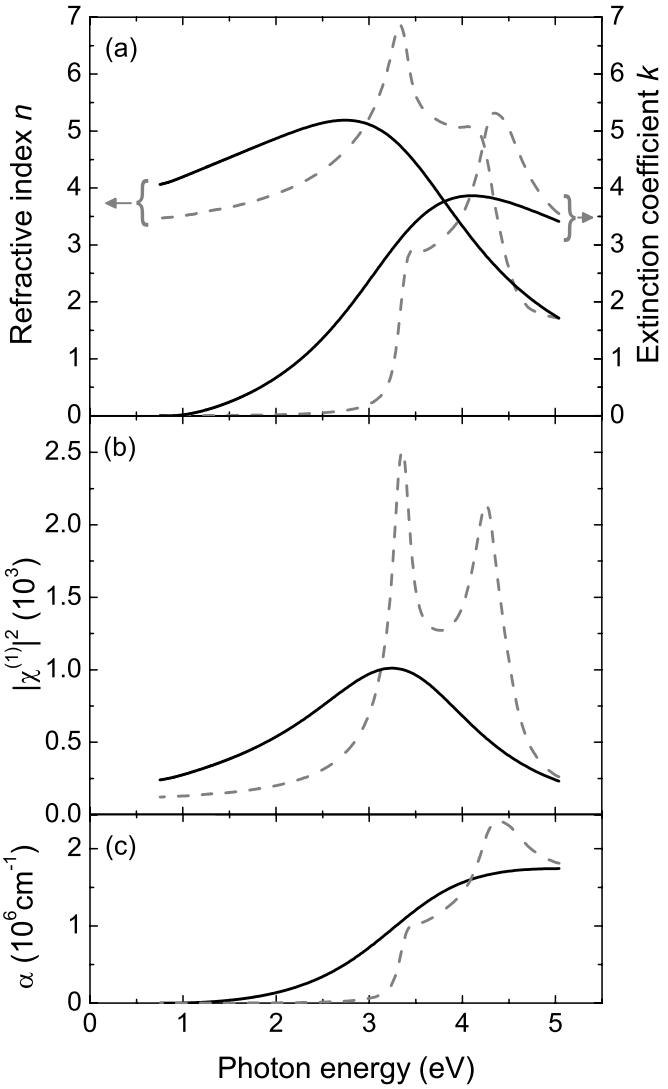

FIG. 2. Spectroscopic ellipsometry data as a function of photon energy for *c*-Si (dashed lines) and *a*-Si layers (solid lines). (a) Refractive index and extinction coefficient. (b) Linear susceptibility squared. (c) Absorption coefficient. Ar^+-ion energies of 70, 200, and 1000 eV have been used to generate the *a*-Si layers.

E_0' and E_1 critical points and the latter to the E_2 critical point of direct optical bandgap transitions in the bulk of the material.[21] The width of the single feature in $|\chi^{(1)}|^2$ of the *a*-Si layers reflects a broader distribution of optical transitions, as expected because of the larger amount of disorder in this material as compared to *c*-Si.[29] The absorption coefficient of *c*-Si and the *a*-Si layers is derived from the extinction coefficient and is shown as a function of photon energy in Fig. 2(c). It can be seen that in the *a*-Si the absorption of radiation increases with increasing photon energy.

The *a*-Si layer thickness and the surface roughness as obtained from the SE measurements are shown in Table I. The thickness of the generated *a*-Si layers increases with increasing ion energy, as a result of the larger penetration depth of more energetic ions. The surface roughness of the *a*-Si layers is comparable to the surface roughness of the initial *H* terminated Si(100). For comparison, the *a*-Si layer thickness derived from molecular dynamics (MD) simulations by Humbird *et al.* are given.[3] The values obtained by experiment and by MD simulations are comparable.

TABLE I. Layer thickness and surface roughness of the *a*-Si layers generated by Ar^+-ion bombardment as obtained from spectroscopic ellipsometry. For comparison the results obtained from molecular dynamics simulations by Humbird *et al.* (Ref. 3) are also given.

Ion energy (eV)	Layer thickness (Å)	Surface roughness (Å)	Simulated layer thickness (Å)
70	15.5	5.0	7 to 8
200	20.1	2.9	15
1000	57.8	7.2	—

IV. SECOND-HARMONIC GENERATION RESULTS

A. SH response to ion bombardment

In Fig. 3 the real time SH response of *H* terminated Si(100) subjected to 70 eV Ar^+-ion bombardment is shown. The experiment was carried out at a SH photon energy of 3.31 eV. At the onset of the ion bombardment, at $t=0$ s, the SHG signal immediately responds and increases rapidly, reaching a steady-state value that is an order of magnitude higher than the initial value within an ion dose on the order of a few ML. When the ion bombardment is terminated at $t=600$ s the SHG intensity decreases, however both the rate and the absolute value of the drop in signal are lower compared to the rate and magnitude of the initial increase. The decreasing SHG signal has not reached a steady-state yet

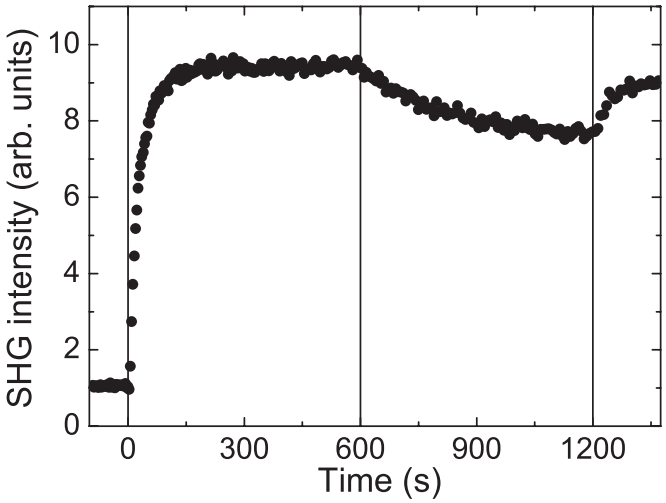

FIG. 3. Real time SHG intensity generated at *H* terminated Si(100) subjected to bombardment with 70 eV Ar^+ ions at a flux of ~0.07 ML/s. At $t=0$ s the Ar^+-ion bombardment is switched on, at $t=600$ s the bombardment is switched off, and at $t=1200$ s the bombardment is switched on again. The SH photon energy is 3.31 eV and both the fundamental and the SH radiation are *p* polarized.

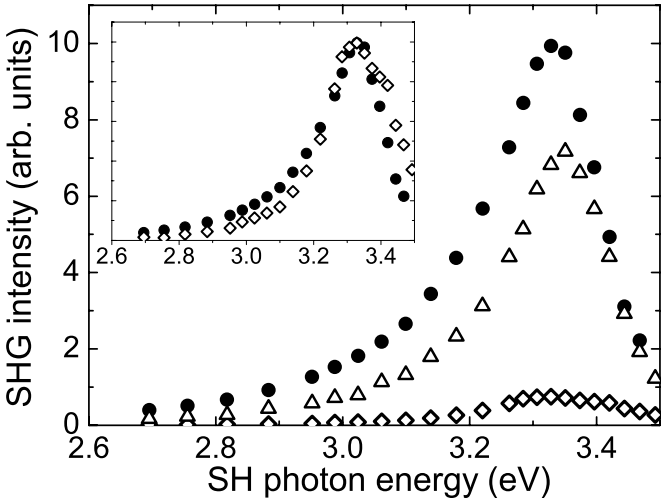

FIG. 4. SHG intensity generated at *H* terminated Si(100) before (open diamonds), during (closed circles) and 24 h after (open triangles) bombardment with 70 eV Ar^+ ions as a function of the SH photon energy for *p* polarized fundamental and SH radiation. In the inset the SHG spectrum before ion bombardment is rescaled to facilitate comparison with the spectrum during Ar^+-ion bombardment.

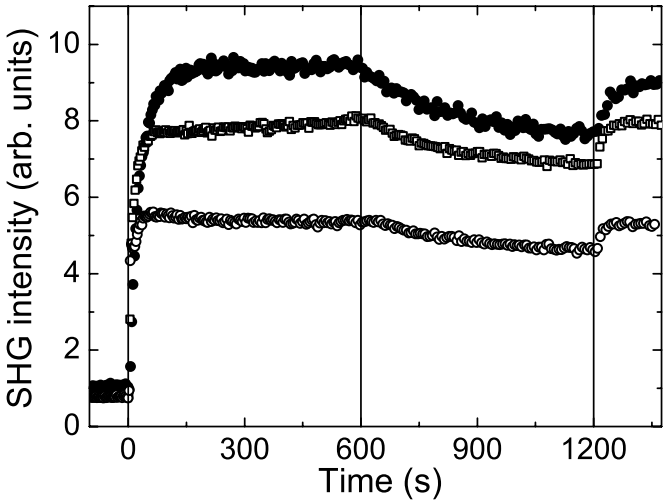

FIG. 5. Real time SHG intensity generated at *H* terminated Si(100) subjected to bombardment with 70 eV (closed circles), 200 eV (open squares), and 1000 eV (open circles) Ar^+ ions at fluxes of ~0.07 ML/s. At $t=0$ s the Ar^+-ion bombardment is switched on, at $t=600$ s the bombardment is switched off, and at $t=1200$ s the bombardment is switched on again. The SH photon energy is 3.31 eV and both the fundamental and the SH radiation are *p* polarized.

when at $t=1200$ s the ion beam is switched on again. The signal returns to about the same steady-state level as during the first exposure to ion bombardment.

The SHG response of the ion etching system has been characterized not only in real time, but also spectroscopically. SHG spectra measured under steady-state conditions before, during, and 24 h after 70 eV Ar^+-ion bombardment of *H* terminated Si(100) are shown in Fig. 4. The spectrum obtained for *H* terminated Si(100) prior to ion bombardment displays a maximum at a SH photon energy of ~3.33 eV and is very similar to spectra reported in the literature.[16,18] When subjecting the *H* terminated Si(100) to 70 eV Ar^+ ions, the spectral feature in the SHG response increases in amplitude by an order of magnitude, in agreement with the real time measurements, and its maximum shifts slightly to lower energies. The inset in Fig. 4 shows that the shape of the spectra before and during ion bombardment is quite similar, however the increase in the SHG signal is more pronounced for SH photon energies below ~3.2 eV than for higher SH photon energies. Repeating the measurement of the SHG spectrum 24 h after stopping the ion bombardment, we observe a slight decrease of the amplitude. However, the amplitude is still considerably larger than in the initial spectrum measured on the pristine *H* terminated Si. In addition, the spectral feature measured 24 h after ion bombardment has shifted to higher photon energies compared to the spectra before and during bombardment.

When comparing the spectroscopic results in Fig. 4 with the real time data in Fig. 3, it is seen that the steady-state value at 3.31 eV in the spectrum 24 h after bombardment is lower than the SHG signal measured in real time 600 s after switching off the ion beam. This is consistent with the observation that the SHG signal has not reached a steady-state at $t=1200$ s in Fig. 3.

B. Dependence on ion energy

In addition to measurements with 70 eV Ar^+ ions, ion etching experiments have been carried out with 200 eV and 1000 eV ions at the same fluence of 0.07 ML/s to investigate the influence of the ion energy on the SHG signal. In Fig. 5 the real time SHG response at a SH photon energy of 3.31 eV of *H* terminated Si(100) before, during, and after bombardment with 200 and 1000 eV ions is shown, together with the results obtained for 70 eV ions. The overall trends are comparable for all ion energies; at the onset of the ion bombardment the SHG signal increases rapidly, when the ion beam is switched off the signal decreases, and when the ion beam is switched on again the signal returns to about the same value as during the initial bombardment. However, the magnitude of the SHG signal is lower and the rate at which the SHG signal increases at the onset of the bombardment is higher when using more energetic ions.

Figure 6 shows the SHG spectra measured under steady-state conditions during bombardment of *H* terminated Si(100) with 70, 200, and 1000 eV ions. As can be seen in Fig. 6, bombarding the *c*-Si with more energetic ions results in a different SHG spectrum. At the high photon energy range in the SHG spectrum the intensity is lower for a more energetic ion bombardment, corresponding to the real time observations shown in Fig. 5, while the SHG intensity at photon energies below ~3.1 eV is similar for all applied ion energies. The peak positions of the resonant features seem to shift slightly to lower photon energies for higher ion energies.

C. XeF_2 dosing

To gain more insight into the spatial origin of the SHG signal from the *a*-Si/*c*-Si system, experiments have been

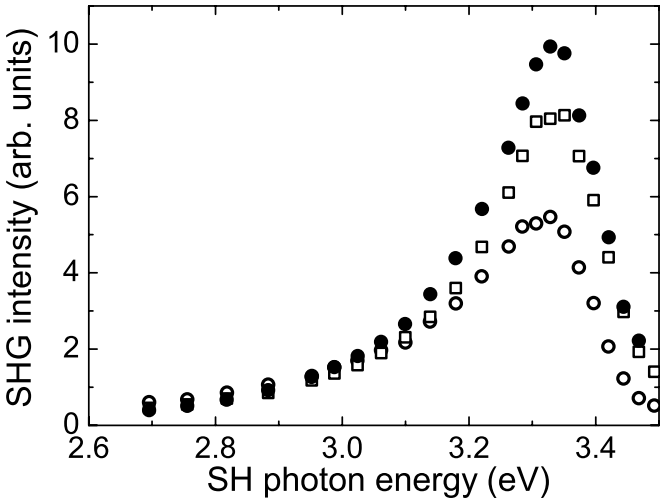

FIG. 6. SHG intensity as a function of the SH photon energy generated at *H* terminated Si(100) during bombardment with Ar^+ ions at energies of 70 eV (closed circles), 200 eV (open squares), and 1000 eV (open circles). Both the fundamental and SH radiation are *p* polarized.

performed in which the surface properties of the *a*-Si were modified. For this purpose *a*-Si layers generated by ion bombardment were, after ending the ion exposure, subjected to a small dose of XeF_2 to terminate the surface with fluorine. In all XeF_2 dosing experiments the dose was limited to prevent substantial spontaneous etching and surface roughening, as was verified by separate SE and QMS experiments. The influence of XeF_2 exposure has been studied in real time and in spectroscopic SHG experiments. Figure 7(a) shows the real time SHG response at a SH photon energy of 3.31 eV of *H* terminated Si(100) that is bombarded with 70 eV Ar^+ ions for 600 s, while at 330 and 460 s after ending the ion bombardment the sample is exposed to a beam of XeF_2 for a period of 30 and 60 s, respectively. The total dose of XeF_2 was ~30 ML from which it can be estimated that at most 1 ML of Si has been removed after the short exposures.[24,26] In Fig. 7(b) the QMS signal due to XeF^+ obtained during the same experiment is shown. This XeF^+ signal is arising from XeF_2 reflected at the surface of the sample. The fast increase of the SHG signal upon the onset of the ion bombardment and the subsequent decrease after switching off the ion beam is similar to the results presented in Fig. 3 and is illustrative for the reproducibility of the measurements. When the first XeF_2 dose is applied the signal decreases rapidly, while the second dose results in a small additional decrease. Note that the reaction of the SHG signal to the XeF_2 exposure is faster than the reaction of the QMS signal.

Figure 8 shows the spectroscopic SHG response of a layer of *a*-Si generated by 1000 eV Ar^+-ion bombardment of Si(100) that is exposed to a small XeF_2 dose (~400 ML) directly after switching off the ion beam. The SHG spectrum was measured under steady-state conditions. In Fig. 8 the SHG spectrum obtained during 1000 eV ion bombardment is also shown for comparison. The spectrum has clearly changed after XeF_2 dosing. At SH photon energies below ~3.35 eV the SHG intensity decreases, while above ~3.35 eV the intensity increases. Furthermore, the resonant

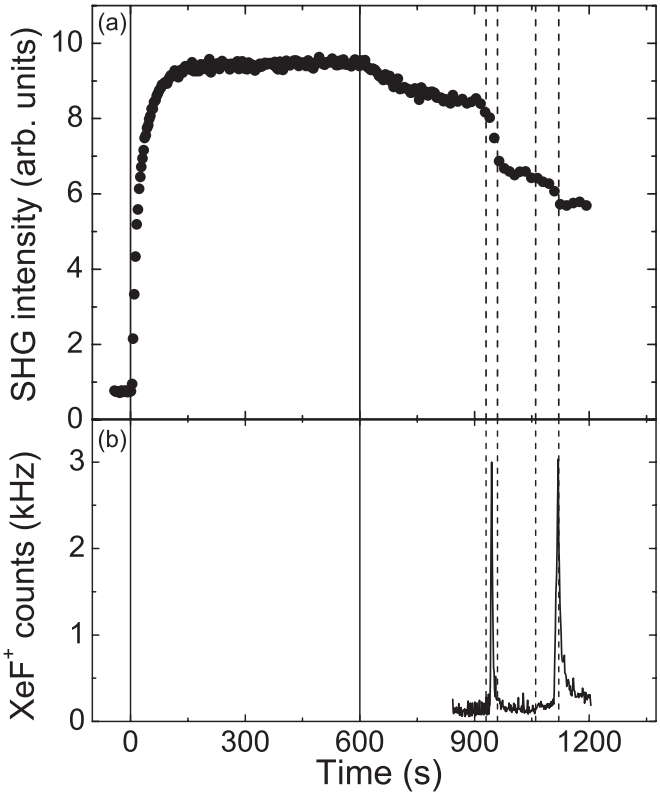

FIG. 7. (a) Real time SHG response of *H* terminated Si(100) (closed circles) bombarded with 70 eV Ar^+ ions at a flux of ~0.07 ML/s followed by two small doses of XeF_2 (in total ~30 ML). Between $t=0$ s and $t=600$ s the sample is exposed to ion bombardment. Between $t=930$ s and $t=960$ s and between $t=1060$ s and 1120 s the XeF_2 beam is switched on. The SH photon energy is 3.31 eV and both the fundamental and the SH radiation are *p* polarized. (b) The count rate due to XeF^+ as measured with the quadrupole mass spectrometer (QMS) during dosing.

feature narrows, has a more symmetric appearance, and its maximum shifts to a higher photon energy after XeF_2 dosing.

V. DISCUSSION

The increase in the spectral features during ion bombardment compared to the spectrum of the initial *H* terminated Si(100) as well as the subsequent decrease in the spectrum measured 24 h after bombardment (both shown in Fig. 4) are more pronounced for SH photon energies below ~3.2 eV than for higher SH photon energies. These observations indicate that the SHG response during ion bombardment originates from multiple sources. These sources of SHG can differ microscopically (e.g., due to different bonding configurations) but can also have different spatial origins. Since the ion bombardment creates a multilayer system, the SHG signal might be generated at different locations in the multilayer system: at the surface of the *a*-Si layer, at the buried interface between the *a*-Si and the underlying *c*-Si, and/or in the bulk of the *a*-Si (e.g., by quadrupole terms). In this section we will first present a hypothesis for the origin of the SHG signal generated during ion bombardment of *c*-Si.

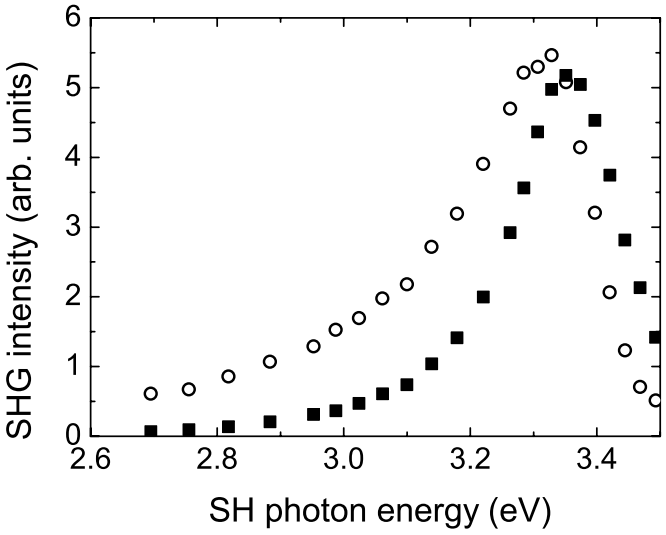

FIG. 8. SHG intensity as a function of the SH photon energy generated at *H* terminated Si(100) during bombardment with 1000 eV Ar^+ ions (open circles) and after subsequent ~400 ML XeF_2 dosing (closed squares) for *p* polarized fundamental and SH radiation.

Next we will use a critical point model to analyze the SHG spectra in more detail to provide more evidence for this hypothesis.

A. Interface contribution

The SHG response is lower at the high photon energy range of the spectra measured during bombardment with more energetic Ar^+ ions, as shown in Fig. 6. Since the results of the SE experiments presented in Fig. 2 showed that the linear optical properties of the *a*-Si layers generated by ions with different energies are very similar it is not plausible that differences in the *a*-Si layer structure are causing the deviations in the spectra. A major difference between the *a*-Si layers generated using different ion energies, however, is the thickness. As indicated by the SE measurements, the thickness is larger for *a*-Si layers generated by more energetic ions. Therefore, it is more likely that the differences in the SH spectra reflect the spatial origin of the SHG signal. The SE data also show that SH radiation propagating through the *a*-Si can be absorbed considerably. Trivially, radiation propagating through thicker *a*-Si layers will be attenuated more. In addition, the SE data show that the absorption by the *a*-Si increases with increasing photon energy, particularly within the applied SH photon energy. This indicates that propagation of SH radiation through the *a*-Si is causing the lower SHG response at the high photon energy range of the spectra obtained for higher ion energies.

We conclude that the SHG signal is likely to be, at least partially, generated at the buried interface between the *a*-Si and the *c*-Si. As the resonant features in the SHG spectra decrease with increasing layer thickness it is unlikely that the SHG signal is generated in the bulk of the *a*-Si layer (e.g., by quadrupole terms). Also the bulk of the underlying *c*-Si is unlikely to contribute significantly to the SHG signal, as the response of the *H* terminated Si prior to ion bombardment was an order of magnitude lower than during bombardment.

B. Surface contribution

The XeF_2 dosing experiments reported in Figs. 7 and 8 provide evidence that the SHG signal is not only generated at the buried interface between the *a*-Si and the *c*-Si but also at the surface of the *a*-Si layer. As the XeF_2 doses were limited and no substantial spontaneous etching or roughening occurred, only the surface of the *a*-Si layer was modified. The SHG signal changes significantly and rapidly upon XeF_2 dosing, which indicates that the SHG radiation is also partially generated at the surface. The XeF_2 exposure might either quench a surface contribution or induce a new contribution to the SHG signal. However, the XeF_2 dosing induces a more symmetric and narrower spectral feature than observed during ion etching, which suggests quenching of a surface contribution in the applied photon energy range. The SE measurements indicate that the surface roughness of the *a*-Si layers is limited. Surface roughness is therefore expected not to contribute to the SHG signal significantly.

As mentioned in the experimental section, a contribution to the SHG signal generated at the surface during ion bombardment cannot be caused by contamination from background species, as under these dynamic conditions any surface contamination will immediately be removed by sputtering. The spectrum obtained 24 h after ion bombardment, however, might be influenced by background species.

C. Excitonic model

So far we have discussed that the SHG signal obtained during ion bombardment of *c*-Si might consist of a contribution generated at the interface between *a*-Si and *c*-Si and a contribution at the surface of the *a*-Si layer, whereas bulk contributions are expected not to be significant. To investigate the validity of this hypothesis we have decomposed the SHG spectra into a number of separate contributions using the theory developed by Erley *et al.*[18,30] The spectra can be reproduced with a model for the SHG intensity described by

$$I(2\omega) = \left| \sum_{L} \sum_{\alpha\beta\gamma} A_{L,\alpha\beta\gamma}(\omega,\theta) \chi^{(2)}_{L,\alpha\beta\gamma}(2\omega) \right|^2 I^2_{\mathrm{in}}(\omega), \quad (3)$$

in which the second-order nonlinear susceptibility is approximated by a coherent superposition of critical pointlike resonances with excitonic line shapes,[21] assuming the fundamental radiation is far from any resonance in the system

$$\chi^{(2)}_{L,\alpha\beta\gamma}(2\omega) = \sum_{q} \chi^{(2)}_{L,\alpha\beta\gamma,q}(2\omega) \propto \sum_{q} \frac{h_q e^{i\varphi_q}}{2\omega - \omega_q + i\Gamma_q}. \quad (4)$$

In Eq. (4) ω_q denotes the frequency, Γ_q the linewidth, h_q the (real) amplitude, and φ_q the excitonic phase of resonance q, all being fitting parameters. The indices $\alpha,\beta,\gamma \in \{x,y,z\}$ in Eqs. (3) and (4) refer to a specific tensor component. The subscripts L refer to the spatial origin or location of the resonances. For the present case, SH radiation generated at the surface or at the buried interface of a single layer on a semi-infinite substrate is included in the model, denoted by L

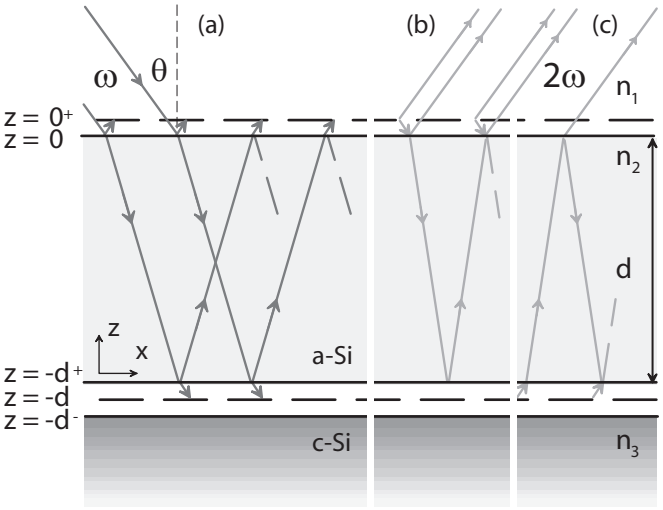

FIG. 9. Two-layer optical model to describe the SHG response of ion bombarded *c*-Si, consisting of vacuum, a layer of *a*-Si with thickness d and a semi-infinite slab of *c*-Si, with refractive indices n_1, n_2, and n_3, respectively. SHG is generated in polarized sheets placed in vacuum gaps at the surface ($z=0^+$) and the buried interface ($z=-d$). Multiple reflections of (a) the fundamental radiation and (b) SH radiation generated at the *a*-Si surface and (c) SH radiation generated at the buried *a*-Si/*c*-Si interface are shown schematically.

$=S,I$. However, it is straightforward to extend the system to more layers.

The complex function $A_{L,\alpha\beta\gamma}(\omega,\theta)$ in Eq. (3) describes the propagation of both the fundamental and the SH radiation through the system and includes linear optical phenomena such as reflection, refraction, and absorption. The latter plays an important role when considering the contribution of a buried interface. Moreover, $A_{L,\alpha\beta\gamma}(\omega,\theta)$ also describes the effects of interference as caused by multiple reflections of the radiation within the system, resulting in frequency dependent phase factors in $A_{L,\alpha\beta\gamma}(\omega,\theta)$. The function $A_{L,\alpha\beta\gamma}(\omega,\theta)$ can be computed from the linear optical properties and the thickness of the different layers in the system. For the present case a two-layer model has been adopted, consisting of a semi-infinite *c*-Si substrate with an *a*-Si layer with thickness d placed on top embedded in vacuum. These layers and the vacuum are referred to as medium 3, 2, and 1, respectively. The geometry is depicted schematically in Fig. 9 with the definition of the coordinate axes. In the calculation of the function $A_{L,\alpha\beta\gamma}(\omega,\theta)$ we follow an approach similar to Koopmans *et al.*[31,32] and Mizrahi and Sipe[33] in which an interface region between two media that generates SH radiation is treated as a polarized sheet placed in an infinitesimal vacuum gap between the two media. Consequently, the interface between the *a*-Si layer and the *c*-Si is assumed to be sharp in our evaluation. The validity of this assumption is supported by transmission electron microscope imaging[8,34] and MD simulations of Ar^+-ion etching of Si[4,35] where the transition from the *a*-Si layer to the *c*-Si was almost atomically sharp but not uniformly flat. In our analysis we use the convention that the local fundamental electric field at a particular interface is also evaluated within the vacuum gap. Other conventions would basically result in a rescaling of the elements of the second-order nonlinear susceptibility tensor $\chi^{(2)}_{L,\alpha\beta\gamma}$ and would not affect the outcome of the analysis.

Consider a fundamental electric field that is polarized along $\hat{e}_{\rm in}$ and is propagating in vacuum at an angle of incidence θ with respect to the film surface given by

$$\mathbf{E}_{\rm in}(\omega,\mathbf{r}) = E_{\rm in}(\omega)e^{i\mathbf{k}_1\cdot\mathbf{r}}\hat{e}_{\rm in}, \tag{5}$$

where $\mathbf{r}=(x,y,z)$ is the position vector and $\mathbf{k}_1$ is the wave vector of the incident fundamental radiation in medium 1, with $\hat{e}_{\rm in}\cdot\mathbf{k}_1=0$. For simplicity, the SH electric field will be evaluated just outside the film in vacuum at $\mathbf{r}=(0,0,0^+)$. To take into account the influence of multiple reflections of the fundamental radiation within the thin layer we define diagonal tensors $\overleftrightarrow{f}_S(\omega)$ and $\overleftrightarrow{f}_I(\omega)$ that relate the local fundamental electric fields at the surface and the interface, evaluated within the vacuum gaps at $z=0^+$ and $z=-d$, to the normalized incident fundamental electric field $\hat{e}_{\rm in}=\mathbf{E}_{\rm in}/|\mathbf{E}_{\rm in}|$

$$\mathbf{e}_L(\omega) = \overleftrightarrow{f}_L\hat{e}_{\rm in}, \tag{6}$$

where

$$\overleftrightarrow{f}_L = f_L^{xx}\hat{x}\hat{x} + f_L^{yy}\hat{y}\hat{y} + f_L^{zz}\hat{z}\hat{z}, \tag{7}$$

with components[32,36]

$$f_S^{\xi\xi} = \frac{(1+r_{12}^{\xi\xi})(1+r_{23}^{\xi\xi}e^{2ik_{2z}d})}{(1-r_{21}^{\xi\xi}r_{23}^{\xi\xi}e^{2ik_{2z}d})}, \tag{8}$$

$$f_I^{\xi\xi} = \frac{(1+r_{12}^{\xi\xi})(1+r_{23}^{\xi\xi})e^{ik_{2z}d}}{(1-r_{21}^{\xi\xi}r_{23}^{\xi\xi}e^{2ik_{2z}d})}, \tag{9}$$

where $\xi\in\{x,y,z\}$. The different tensor components in Eqs. (8) and (9) are related to the Fresnel coefficients r_{ij}^p and r_{ij}^s, which describe the reflection of light propagating from medium i to j for reflection of *p*- and *s* polarized radiation, $-r_{ij}^{xx}=r_{ij}^{zz}=r_{ij}^p$ and $r_{ij}^{yy}=r_{ij}^s$. The SH radiation also encounters multiple reflections within the thin layer. Since these reflections are the same as for the fundamental radiation, Eqs. (7)–(9) are also valid for the SH radiation. For clarity, the tensors describing multiple reflections of the SH radiation will be shown in upper case. In analogy with the fundamental case, the SH electric field at $z=0^+$ with polarization vector $\hat{e}_{\rm out}$ can be related to the SH field generated at the surface or interface by

$$\mathbf{e}_L(2\omega) = \hat{e}_{\rm out}\cdot\overleftrightarrow{F}_L. \tag{10}$$

Equation (3) can now be rewritten as

$$I(2\omega) = \frac{2\omega^2}{\varepsilon_0 c^3\cos^2\theta}\left|\sum_L \mathbf{e}_L(2\omega)\cdot\overleftrightarrow{\chi}_L^{(2)}(2\omega):\mathbf{e}_L(\omega)\mathbf{e}_L(\omega)\right|^2 I_{\rm in}^2(\omega), \tag{11}$$

where the different elements of $\overleftrightarrow{\chi}_L^{(2)}$ are given by Eq. (4) and $I_{\rm in}(\omega)$ is the intensity of the incident fundamental radiation. The SHG intensity in Eq. (11) is evaluated in vacuum, which

can be replaced by an arbitrary dispersive medium i by exchanging $\cos^2\theta$ in the denominator of Eq. (11) by $n_i(2\omega)n_i^2(\omega)\cos^2\theta_i(2\omega)$.

The spectra presented in this paper were all obtained for p polarized fundamental and SH radiation. For an amorphous medium such as a-Si, it is to be expected that for this polarization combination the tensor components $\chi^{(2)}_{zzz}$, $\chi^{(2)}_{zxx}$, and $\chi^{(2)}_{xxz}$ contribute to the SHG response.[37,38] However, the contribution of the tensor components $\chi^{(2)}_{zxx}$ and $\chi^{(2)}_{xxz}$ is expected to be minimal as the propagation function for these tensor components is much lower. Quantitatively, $|A_{L,\alpha\beta\gamma}(\omega,\theta)|^2$ is at least two orders of magnitude lower for these tensor components, which is mainly related to the angle of incidence at the sample of 74° that induces a large z component in the electric fields. This is supported by experiments we carried out for s polarized fundamental and p polarized SH radiation and for fundamental radiation with equal p and s polarized components and s polarized SH radiation. The SHG response obtained for these polarization combinations appeared to be roughly a factor of 70 lower than for p polarized fundamental and SH radiation. For these polarization combinations the tensor components that are expected to contribute to the SHG response are $\chi^{(2)}_{zyy}$ and $\chi^{(2)}_{yyz}$, respectively, where $\chi^{(2)}_{zyy}$ is equal to $\chi^{(2)}_{zxx}$ and $\chi^{(2)}_{yyz}$ is equal to $\chi^{(2)}_{xxz}$. The magnitude of the corresponding functions $A_{L,\alpha\beta\gamma}(\omega,\theta)$ is comparable for these four tensor components. Therefore, in the applied geometry, the SHG signal for p polarized fundamental and SH radiation is governed by $\chi^{(2)}_{zzz}$.

Consequently, to minimize the number of curve fitting parameters we have only taken tensor elements $\chi^{(2)}_{S,zzz}$ and $\chi^{(2)}_{I,zzz}$ into account for the analysis of the spectra. Both tensor elements are modeled by a single resonance. Hence, the spectra are curve fitted using seven parameters, being the resonance frequencies, linewidths, amplitudes of both resonances, and a single phase difference, since only the relative phase between both contributions influences the spectrum. The curve fitting has been carried out with a commercial software package, Mathematica 5.2, using a Levenberg-Marquardt least square algorithm. The corresponding functions describing the propagation through the system, $A_{S,zzz}$ and $A_{I,zzz}$, are calculated using the linear optical properties and the thickness of the amorphized layers as obtained with SE (Fig. 2 and Table I).

To avoid the curve fitting procedure to be stalled at a local minimum yielding unphysical results, an iterative fitting procedure has been applied. The procedure is started by temporarily fixing the resonance energy of the surface contribution at 3.2 eV, the resonance energy of the linear susceptibility squared of the bulk a-Si, while performing a least square fit using the other six parameters. Then the amplitude, frequency, and linewidth of the interface contribution were fixed and the parameters of the surface contribution and the phase difference were included in the fitting run. Finally, the latter step was repeated to optimize the interface contribution while keeping the surface contribution fixed. It was verified that the parameters did not vary anymore outside their error values. More important, the SHG spectra could not be reproduced with the excitonic model when including only a single resonance either at the surface or the buried interface in the curve fitting procedure.

D. Results excitonic model

Figure 10 shows the fits to the SHG spectra obtained during 70 , 200, and 1000 eV Ar^+-ion bombardment and after XeF_2 dosing. The individual resonances (without propagation correction $A_{L,zzz}$) at the interface between the a-Si and the c-Si and at the surface of the a-Si layer are also displayed. The fits reproduce the spectra very well and confirm the presence of sources of SHG at the buried interface and at the a-Si surface. An overview of the resulting curve fitting parameters can be found in Table II. The contribution at the buried interface is a sharp resonance at a SH photon energy of 3.36 eV and a linewidth of 0.1 eV. This contribution is the same for all spectra in Fig. 10 and does, consequently, not depend on the applied ion energy and is not influenced by the XeF_2 dosing. In Fig. 10(e) the linear susceptibilities squared for the a-Si layers and c-Si are displayed for the appropriate photon energy range (see also Fig. 2). The resonance of the SHG contribution at 3.36 eV corresponds very well to the resonance at 3.37 eV in the linear susceptibility squared of the c-Si, indicating that both resonances have a common microscopic origin. Hence, the SHG contribution at the buried interface between a-Si and c-Si is most likely generated by the E_0'/E_1 transitions between bulk electronic states in the c-Si that are modified due to the vicinity of the interface, similar as reported for c-Si.[14,16,18]

The contribution at the surface consists of a broad resonance at a SH photon energy of (3.16 ± 0.02) eV with a linewidth of 0.5 eV and is much weaker. Nevertheless, the influence of this additional resonance is significant, as due to the propagation of the radiation through the a-Si/c-Si system the surface contribution is relatively enhanced with respect to the interface contribution. This additional resonance seems to depend weakly on the applied ion energy but is still very similar for the three spectra in Figs. 10(a)–10(c). In contrast, for the spectrum after XeF_2 dosing [Fig. 10(d)] the surface contribution has almost disappeared and the SHG response originates mainly from the resonance at the buried interface. When comparing the surface contribution to the SHG signal for all ion energies with the linear optical properties of the layers in Fig. 10(e), it becomes clear that this contribution resembles the broad resonance in the linear susceptibility squared of the a-Si layers. This indicates that this additional contribution to the SHG signal is originating from optical transitions related to Si-Si bonds at the a-Si surface.

We have recently reported spectroscopic SHG experiments with the same laser system on hydrogenated amorphous silicon (a-Si:H) films deposited with hot-wire chemical vapor deposition.[39,40] The a-Si:H was deposited on fused silica substrates from which no SHG signal could be detected. The SHG spectrum reflected a broad feature, which, although being at the edge of the photon energy range, seemed to have a maximum at a SH photon energy of ~3.4 eV. The broad spectrum for the a-Si:H films is different from the present spectra as measured during ion bombardment. However, apart from a somewhat higher peak energy, it corresponds well to the broad contribution due to the a-Si surface obtained after decomposing the present spectra with the excitonic model. Similar to the linear case, the broadness of the SHG contribution originating from the

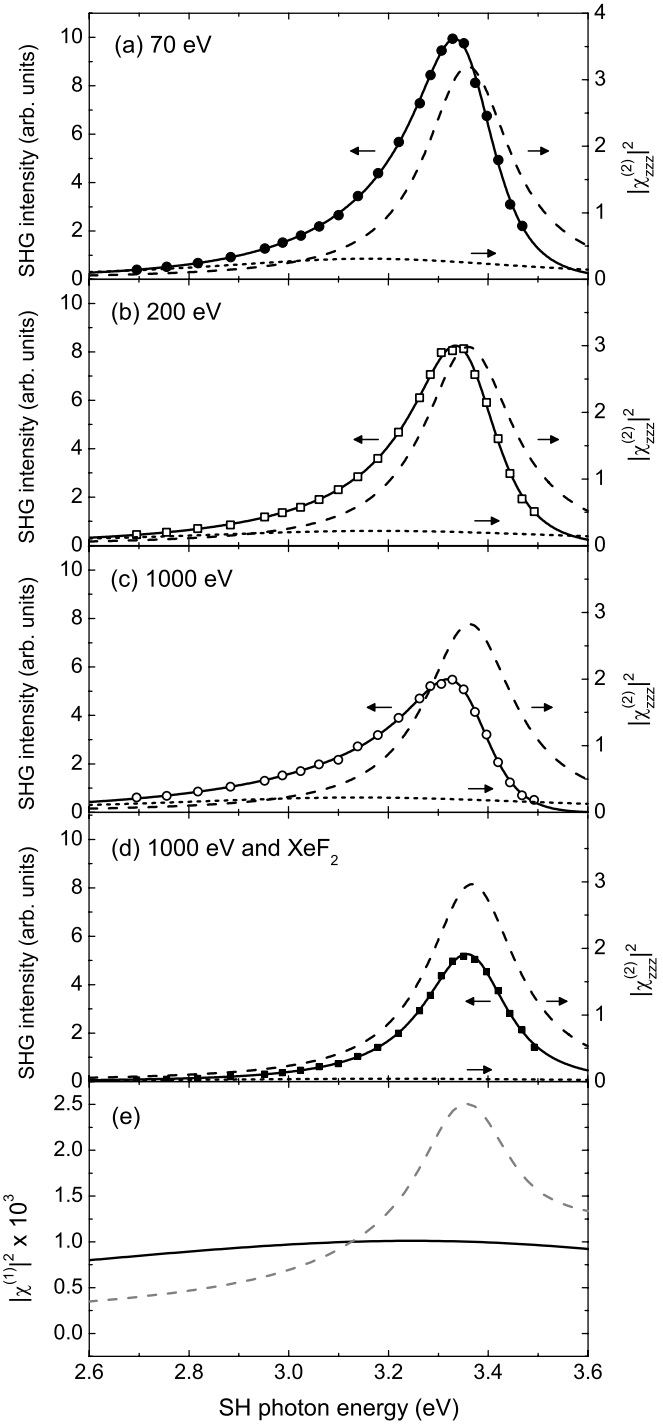

FIG. 10. Experimental (symbols) and simulated (solid lines) SHG spectra measured at *H* terminated Si(100) during bombardment with Ar^+ ions at energies of (a) 70 eV, (b) 200 eV, and (c) 1000 eV and (d) after XeF_2 dosing directly after 1000 eV ion bombardment. The solid lines in (a)–(d) are fits to the data using a superposition of two CP-like resonances. The dashed and the dotted lines represent the individual resonances $\chi^{(2)}_{I,zzz}$ at the buried interface between *a*-Si and *c*-Si and $\chi^{(2)}_{S,zzz}$ at the *a*-Si surface, respectively, without the propagation functions $A_{L,zzz}$ taken into account. In (e) the linear susceptibility squared as in Fig. 2(b) is given in the same photon energy range as the SHG spectra.

a-Si surface, compared to the *c*-Si-like resonance at the interface reflects the disorder in the *a*-Si.

Although the SHG spectra obtained during bombardment at different ion energies were significantly different, the decomposition of the spectra with the excitonic model resulted in the same resonances at the buried interface and comparable resonances at the surface. Also the spectrum after XeF_2 dosing is predominantly generated by the same interface contribution. The differences in the measured spectra are caused mainly by the propagation of the fundamental and the SH radiation through the *a*-Si/*c*-Si system and are consequently described by the factors $A_{S,zzz}$ and $A_{I,zzz}$ in Eq. (3). As the model showed to be a valid description of the SHG response of the *a*-Si/*c*-Si system, it indirectly validates the assumption that the interface between the *a*-Si layer and the *c*-Si is sharp. Accordingly, the interface can effectively be described by a two-layer model with a sharp transition. Moreover, the results obtained with the excitonic model support the assumption that bulk quadrupole terms in *a*-Si are not likely to contribute substantially to the signal. These terms would most likely result in a resonance close to the bulk value of *a*-Si of ~3.2 eV. However, the contribution that is observed at this SH photon energy is quenched by surface modification with XeF_2, while the remaining contribution is located at 3.36 eV.

After switching off the ion bombardment the SHG signal decreases, as seen in the real time data and in the spectrum obtained 24 h after ion bombardment (Fig. 4). This spectrum can also be curve fitted with a contribution at the buried interface and one at the surface (not shown). However, both contributions are lower than in the spectra obtained during ion bombardment. Several phenomena can cause the decrease in SHG signal. The lower response at the interface might be caused by reconstruction of the *a*-Si after ending the ion bombardment, while the lower surface contribution might indicate a contamination of the *a*-Si surface by background species in the vacuum chamber such as water and oxygen. Conversely, as discussed in the experimental section, the SHG spectra obtained during ion bombardment are not influenced by background species due to continuous sputtering of the outermost surface layer.

E. Microscopic origin of the SHG signal

Numerous spectroscopic SHG studies of clean *c*-Si[14–20] and the technologically important Si-SiO_2 system[10] have been reported in the literature. Also in these studies resonant features were observed near the E_0'/E_1 critical point energies of ~3.4 eV. These features have been suggested to originate from a two-photon resonance due to distorted Si-Si bonds at the selvedge of the clean Si surface and at the Si-SiO_2 interface.[14] Also electric-field-induced SHG (EFISH) has been reported to have an important contribution to the SHG signal at a SH photon energy of ~3.4 eV for these systems.[18] The EFISH contribution is caused by the presence of a dc-electric field in the subsurface or subinterface space-charge region due to band bending at the clean *c*-Si surface and at the Si-SiO_2 interface.

For the present case, it is not straightforward to give a conclusive explanation for the microscopic origin of both

TABLE II. The parameter values of the critical point resonances at the interface (I) and the surface (S) obtained from the fits to the SHG spectra obtained during bombardment of H terminated Si(100) with 70, 200, and 1000 eV Ar^+ ions and after XeF_2 dosing directly after 1000 eV Ar^+-ion bombardment.

Ion energy (eV)	h_I (arb.units)	$\hbar\omega_I$ (eV)	$\hbar\Gamma_I$ (eV)	h_S (arb. units)	$\hbar\omega_S$ (eV)	$\hbar\Gamma_S$ (eV)	φ (π rad)
70	0.187±0.004	3.359±0.001	0.104±0.002	0.232±0.009	3.16±0.03	0.42±0.03	1.24±0.01
200	0.190±0.003	3.361±0.001	0.110±0.001	0.26±0.02	3.18±0.04	0.55±0.06	1.26±0.01
1000	0.183±0.005	3.363±0.001	0.109±0.002	0.25±0.01	3.14±0.02	0.54±0.04	1.45±0.01
1000 and XeF_2	0.186±0.002	3.368±0.001	0.108±0.001	0.102±0.07	3.20±0.08	0.49±0.05	1.32±0.01

contributions to the SHG response. It is very likely that the SHG contribution at the buried interface between a-Si and c-Si is related to E_0'/E_1 transitions between bulk electronic states in the c-Si modified due to the vicinity of the interface and, similarly, that the surface contribution is caused by bulklike transitions in a-Si modified by the presence of the a-Si surface. Whether or not these modifications yield distorted Si-Si bonds or EFISH effects, as proposed for c-Si, is not yet clear from our data. Distorted bonds are known to shift the energy of interband transitions. The difference between the E_0'/E_1 critical point energy of bulk c-Si at 3.37 eV and the energy of the SHG interface contribution of 3.36 eV seems to be not significant. The difference between the peak energy of the linear susceptibility of the a-Si bulk at ~3.2 eV and the SHG contribution at the a-Si surface at ~3.16 eV is somewhat larger, however not conclusive. The possible influence of EFISH effects, caused by local electric fields at the a-Si/c-Si interface or a-Si surface, cannot be distinguished from other effects. Varying the doping level of the Si(100) substrates might influence any space charge, if present, and could give more insight into the possible contribution of EFISH.

VI. CONCLUSIONS

The SHG response of H terminated Si(100) has been studied during bombardment with 70, 200, and 1000 eV Ar^+ ions, both in real time at the onset of bombardment and spectroscopically under steady-state conditions. The SHG signal from initially H terminated Si was observed to increase substantially and fast upon Ar^+-ion bombardment. We have shown that the SHG response during ion bombardment consists of two contributions, a main contribution that is caused by E_0'/E_1 transitions between bulk electronic states in the c-Si that are modified due to the vicinity of the interface with the a-Si layer, and an additional contribution that arises from transitions related to Si-Si bonds at the a-Si surface. Both contributions are independent of the applied Ar^+-ion energy, while the surface contribution is almost completely quenched upon XeF_2 exposure. The results reported have demonstrated that SHG is a very useful technique to obtain insight into the surface and interface properties of silicon during ion etching. The potential of the SHG technique to study plasma etching of Si will be explored further in future XeF_2 etching[41] and Ar^+-ion assisted XeF_2 etching experiments.

ACKNOWLEDGMENTS

The authors acknowledge fruitful discussions with B. Koopmans and technical assistance from L. H. A. M. van Moll, J. A. C. M. van de Ven, M. J. F. van de Sande, J. F. C. Jansen, A. B. M. Hüsken, and H. M. M. de Jong. This work was supported by the Netherlands Foundation for Fundamental Research on Matter (FOM). The research of W.K. has been made possible by the Royal Netherlands Academy of Arts and Sciences (KNAW).

*Corresponding author. Email address: w.m.m.kessels@tue.nl

[1] J. W. Coburn and H. F. Winters, J. Appl. Phys. **50**, 3189 (1979).
[2] H. F. Winters and J. W. Coburn, Surf. Sci. Rep. **14**, 161 (1992).
[3] D. Humbird and D. B. Graves, Pure Appl. Chem. **74**, 419 (2002).
[4] D. B. Graves and D. Humbird, Appl. Surf. Sci. **192**, 72 (2002).
[5] L. Hanley and S. B. Sinnott, Surf. Sci. **500**, 500 (2002).
[6] J. C. Bean, G. E. Becker, P. M. Petroff, and T. E. Seidel, J. Appl. Phys. **48**, 907 (1977).
[7] L. M. Garverick, J. H. Comfort, T. R. Yew, R. Reif, F. A. Baiocchi, and H. S. Luftman, J. Appl. Phys. **62**, 3398 (1987).
[8] J. G. C. Labanda, S. A. Barnett, and L. Hultman, J. Vac. Sci. Technol. B **16**, 1885 (1998).
[9] Y. R. Shen, *The Principles of Nonlinear Optics* (Wiley, New York, 1984).
[10] G. Lüpke, Surf. Sci. Rep. **35**, 75 (1999).
[11] A. Priem, C. W. van Hasselt, M. A. C. Devillers, and Th. Rasing, Surf. Sci. **352**, 612 (1996).
[12] J. Fang, W. W. Heidbrink, and G. P. Li, J. Appl. Phys. **88**, 2641 (2000).
[13] I. V. Kravetsky, L. L. Kulyuk, A. V. Micu, V. I. Tsytsanu, and I. S. Vieru, J. Non-Cryst. Solids **187**, 227 (1995).
[14] W. Daum, H.-J. Krause, U. Reichel, and H. Ibach, Phys. Rev. Lett. **71**, 1234 (1993).
[15] K. Pedersen and P. Morgen, Phys. Rev. B **52**, R2277 (1995); **53**, 9544 (1996).
[16] U. Höfer, Appl. Phys. A **63**, 533 (1996).
[17] K. Pedersen and P. Morgen, Surf. Sci. **377**, 393 (1997).
[18] J. I. Dadap, Z. Xu, X. F. Hu, M. C. Downer, N. M. Russell, J. G. Ekerdt, and O. A. Aktsipetrov, Phys. Rev. B **56**, 13367 (1997).
[19] T. Suzuki, Phys. Rev. B **61**, R5117 (2000).

[20] Y. Q. An and S. T. Cundiff, Appl. Phys. Lett. **81**, 5174 (2002).
[21] P. Lautenschlager, M. Garriga, L. Viña, and M. Cardona, Phys. Rev. B **36**, 4821 (1987).
[22] S. Haraichi, F. Sasaki, S. Kobayashi, M. Komuro, and T. Tani, J. Vac. Sci. Technol. B **13**, 745 (1995).
[23] T. F. Heinz, M. M. T. Loy, and W. A. Thompson, J. Vac. Sci. Technol. A **3**, 1467 (1985).
[24] G. J. P. Joosten, M. J. M. Vugts, H. J. Spruijt, H. A. J. Senhorst, and H. C. W. Beijerinck, J. Vac. Sci. Technol. A **12**, 636 (1994).
[25] M. J. M. Vugts, G. J. P. Joosten, A. van Oosterum, H. A. J. Senhorst, and H. C. W. Beijerinck, J. Vac. Sci. Technol. A **12**, 2999 (1994).
[26] A. A. E. Stevens and H. C. W. Beijerinck, J. Vac. Sci. Technol. A **23**, 126 (2005).
[27] A. A. E. Stevens, W. M. M. Kessels, M. C. M. van de Sanden, and H. C. W. Beijerinck, J. Vac. Sci. Technol. A **24**, 1933 (2006).
[28] G. E. Jellison, Jr. and F. A. Modine, Appl. Phys. Lett. **69**, 371 (1996).
[29] S. Adachi and H. Mori, Phys. Rev. B **62**, 10158 (2000).
[30] G. Erley, R. Butz, and W. Daum, Phys. Rev. B **59**, 2915 (1999).
[31] B. Koopmans, A. Anema, H. T. Jonkman, G. A. Sawatzky, and F. van der Woude, Phys. Rev. B **48**, 2759 (1993).
[32] B. Koopmans, Ph.D. thesis, Rijksuniversiteit Groningen, Groningen, 1993.
[33] V. Mizrahi and J. E. Sipe, J. Opt. Soc. Am. B **5**, 660 (1988).
[34] M. E. Day, M. Delfino, W. Tsai, A. Bivas, and K. N. Ritz, J. Appl. Phys. **74**, 5217 (1993).
[35] D. Humbird, D. B. Graves, A. A. E. Stevens, and W. M. M. Kessels (unpublished).
[36] A. Vasicek, *Optics of Thin Films* (North-Holland, Amsterdam, 1960).
[37] T. F. Heinz, *Nonlinear Effects at Surfaces and Interfaces*, in Nonlinear Surface Electromagnetic Phenomena, edited by H. Ponath and G. Stegeman (Elsevier, Amsterdam, 1991), p. 353.
[38] W. M. M. Kessels, J. J. H. Gielis, I. M. P. Aarts, C. M. Leewis, and M. C. M. van de Sanden, Appl. Phys. Lett. **85**, 4049 (2004).
[39] J. J. H. Gielis, A. A. E. Stevens, P. M. Gevers, H. C. W. Beijerinck, M. C. M. van de Sanden, and W. M. M. Kessels, Phys. Status Solidi C **2**, 3968 (2005).
[40] I. M. P. Aarts, J. J. H. Gielis, M. C. M. van de Sanden, and W. M. M. Kessels, Phys. Rev. B **73**, 045327 (2006).
[41] A. A. E. Stevens, J. J. H. Gielis, P. M. Gevers, M. C. M. van de Sanden, H. C. W. Beijerinck, and W. M. M. Kessels (unpublished).